^{197}Au(n,γ) cross section in the unresolved resonance region

C. Lederer,[1,*] N. Colonna,[2] C. Domingo-Pardo,[3] F. Gunsing,[4] F. Käppeler,[5] C. Massimi,[6] A. Mengoni,[7,8] A. Wallner,[1] U. Abbondanno,[9] G. Aerts,[4] H. Álvarez,[10] F. Álvarez-Velarde,[11] S. Andriamonje,[4] J. Andrzejewski,[12] P. Assimakopoulos,[13,†] L. Audouin,[14] G. Badurek,[15] M. Barbagallo,[2] P. Baumann,[16] F. Bečvář,[17] F. Belloni,[9] E. Berthoumieux,[4] M. Calviani,[8] F. Calviño,[18] D. Cano-Ott,[11] R. Capote,[7,19] C. Carrapiço,[20,4] A. Carrillo de Albornoz,[20] P. Cennini,[8] V. Chepel,[21] E. Chiaveri,[8] G. Cortes,[22] A. Couture,[23] J. Cox,[23] M. Dahlfors,[8] S. David,[14] I. Dillmann,[5] R. Dolfini,[24] W. Dridi,[4] I. Duran,[10] C. Eleftheriadis,[25] M. Embid-Segura,[11] L. Ferrant,[14,†] A. Ferrari,[8] R. Ferreira-Marques,[21] L. Fitzpatrick,[8] H. Frais-Koelbl,[7] K. Fujii,[9] W. Furman,[26] I. Goncalves,[21] E. González-Romero,[11] A. Goverdovski,[27] F. Gramegna,[28] E. Griesmayer,[7] C. Guerrero,[11] B. Haas,[29] R. Haight,[30] M. Heil,[31] A. Herrera-Martinez,[8] M. Igashira,[32] S. Isaev,[14] E. Jericha,[15] Y. Kadi,[8] D. Karadimos,[13] D. Karamanis,[13] M. Kerveno,[16] V. Ketlerov,[26] P. Koehler,[33] V. Konovalov,[25] E. Kossionides,[34] M. Krtička,[17] C. Lampoudis,[25,4] H. Leeb,[15] A. Lindote,[21] I. Lopes,[21] R. Losito,[8] M. Lozano,[19] S. Lukic,[16] J. Marganiec,[12] L. Marques,[20] S. Marrone,[2] T. Martínez,[11] P. Mastinu,[28] E. Mendoza,[11] P. M. Milazzo,[9] C. Moreau,[9] M. Mosconi,[5] F. Neves,[21] H. Oberhummer,[15] S. O'Brien,[23] M. Oshima,[35] J. Pancin,[4] C. Papachristodoulou,[13] C. Papadopoulos,[36] C. Paradela,[10] N. Patronis,[13] A. Pavlik,[1] P. Pavlopoulos,[37] L. Perrot,[4] M. T. Pigni,[15] R. Plag,[5] A. Plompen,[38] A. Plukis,[4] A. Poch,[22] J. Praena,[19] C. Pretel,[22] J. Quesada,[19] T. Rauscher,[39] R. Reifarth,[30] M. Rosetti,[40] C. Rubbia,[24] G. Rudolf,[16] P. Rullhusen,[38] J. Salgado,[20] C. Santos,[20] L. Sarchiapone,[8] R. Sarmento,[20] I. Savvidis,[25] C. Stephan,[14] G. Tagliente,[2] J. L. Tain,[3] D. Tarrío,[10] L. Tassan-Got,[14] L. Tavora,[20] R. Terlizzi,[2] G. Vannini,[6] P. Vaz,[20] A. Ventura,[40] D. Villamarin,[11] V. Vlachoudis,[8] R. Vlastou,[36] F. Voss,[5] S. Walter,[5] H. Wendler,[8] M. Wiescher,[23] and K. Wisshak[5]

(n_TOF Collaboration)[‡]

[1]*University of Vienna, Faculty of Physics, Vienna, Austria*
[2]*Istituto Nazionale di Fisica Nucleare, Bari, Italy*
[3]*Instituto de Física Corpuscular, CSIC-Universidad de Valencia, Valencia, Spain*
[4]*CEA/Saclay, IRFU, Gif-sur-Yvette, France*
[5]*Karlsruhe Institute of Technology (KIT), Campus Nord, Institut für Kernphysik, Karlsruhe, Germany*
[6]*Dipartimento di Fisica, Università di Bologna, and Sezione INFN di Bologna, Bologna, Italy*
[7]*Nuclear Data Section, International Atomic Energy Agency (IAEA), Vienna, Austria*
[8]*CERN, Geneva, Switzerland*
[9]*Istituto Nazionale di Fisica Nucleare, Trieste, Italy*
[10]*Universidade de Santiago de Compostela, Santiago de Compostela, Spain*
[11]*Centro de Investigaciones Energeticas Mediosample-independentales y Tecnologicas, Madrid, Spain*
[12]*University of Lodz, Lodz, Poland*
[13]*University of Ioannina, Ioannina, Greece*
[14]*Centre National de la Recherche Scientifique/IN2P3, IPN, Orsay, France*
[15]*Atominstitut der Österreichischen Universitäten, Technische Universität Wien, Vienna, Austria*
[16]*Centre National de la Recherche Scientifique/IN2P3, IReS, Strasbourg, France*
[17]*Charles University, Prague, Czech Republic*
[18]*Universidad Politecnica de Madrid, Madrid, Spain*
[19]*Universidad de Sevilla, Seville, Spain*
[20]*Instituto Tecnológico e Nuclear (ITN), Lisbon, Portugal*
[21]*LIP-Coimbra and Departamento de Fisica da Universidade de Coimbra, Coimbra, Portugal*
[22]*Universitat Politecnica de Catalunya, Barcelona, Spain*
[23]*University of Notre Dame, Notre Dame, Indiana 46556, USA*
[24]*Università degli Studi Pavia, Pavia, Italy*
[25]*Aristotle University of Thessaloniki, Thessaloniki, Greece*
[26]*Frank Laboratory of Neutron Physics, Joint Institute for Nuclear Research, Dubna, Russia*
[27]*Institute of Physics and Power Engineering, Kaluga Region, Obninsk, Russia*
[28]*Laboratori Nazionali di Legnaro, Istituto Nazionale di Fisica Nucleare, Legnaro, Italy*
[29]*Centre National de la Recherche Scientifique/IN2P3, CENBG, Bordeaux, France*
[30]*Los Alamos National Laboratory, Los Alamos, New Mexico 87545, USA*
[31]*GSI Helmholtzzentrum für Schwerionenforschung GmbH, Darmstadt, Germany*
[32]*Tokyo Institute of Technology, Tokyo, Japan*
[33]*Physics Division, Oak Ridge National Laboratory, Oak Ridge, Tennessee 37831, USA*
[34]*NCSR, Athens, Greece*
[35]*Japan Atomic Energy Research Institute, Tokai-mura, Ibaraki, Japan*

[36]*National Technical University of Athens, Athens, Greece*
[37]*Pôle Universitaire Léonard de Vinci, Paris La Défense, France*
[38]*CEC-JRC-IRMM, Geel, Belgium*
[39]*Department of Physics, University of Basel, Basel, Switzerland*
[40]*ENEA, Bologna, Italy*
(Received 19 January 2011; published 17 March 2011)

The cross section of the reaction ^{197}Au(n,γ) was measured with the time-of-flight technique at the n_TOF (neutron time-of-flight) facility in the unresolved resonance region between 5 and 400 keV using a pair of C_6D_6 (where D denotes ^{2}H) liquid scintillators for the detection of prompt capture γ rays. The results with a total uncertainty of 3.9%–6.7% for a resolution of 20 bins per energy decade show fair agreement with the Evaluated Nuclear Data File Version B-VII.0 (ENDF/B-VII.0), which contains the standard evaluation. The Maxwellian-averaged cross section (MACS) at 30 keV is in excellent agreement with the one according to the ENDF/B-VII.0 evaluation and 4.7% higher than the MACS measured independently by activation technique. Structures in the cross section, which had also been reported earlier, have been interpreted as being due to clusters of resonances.

DOI: 10.1103/PhysRevC.83.034608 PACS number(s): 25.40.Lw, 29.30.Hs, 27.80.+w

I. MOTIVATION

The ^{197}Au(n,γ) cross section is an established cross-section standard for thermal neutron energies (at 0.0253 eV) and for the energy range between 0.2 and 2.8 MeV [1]. The evaluation of the standard cross section is based on available experimental data, including absolute measurements and information from relative measurements and from measurements of cross-section ratios. Although the evaluation covers the lower kilo-electron-volt region above the resolved resonance region as well, it is not a recommended standard below 200 keV due to discrepancies of 6%–8% compared to results, which were essentially obtained in two well-designed experiments, a time-of-flight (TOF) measurement at Oak Ridge Electron Linear Accelerator (ORELA) [2,3] and an activation measurement at the Karlsruhe Van de Graaff accelerator [4], which agree within 1.5%.

The TOF measurement of Macklin [2,3] was performed in the energy range from thermal up to 2 MeV with the intention of establishing an accurate (n,γ) cross section for use as a standard. The experiment was carried out with the pulse-height-weighting technique (PHWT) [5] at the 40-m station of the ORELA facility. The data were taken with a sample 0.55 mm in thickness and an energy resolution that increased from 0.25% (full-width half-maximum, FWHM) at 100 keV to 0.8% at 2 MeV. This pioneering effort, which claimed an overall uncertainty of 3.6 to 4.7%, reported also significant structures in the energy region up to about 200 keV.

In the completely different activation measurement at Karlsruhe, neutrons were produced via the ^{7}Li$(p,n)^7$Be reaction at proton energies of 1912 keV [4]. The resulting neutron spectrum is emitted in a forward-peaked cone with an opening angle of 120° and is important for applications in nuclear astrophysics because it corresponds closely to a Maxwell-Boltzmann distribution for a thermal energy of $k_BT = 25$ keV. This spectrum is typical for the slow neutron capture process (s process) of nucleosynthesis, which contributes about half of the natural isotopic abundances between Fe and Bi and occurs during the He burning stages of stellar evolution [6]. The capture cross section of ^{197}Au was measured in this spectrum by irradiation of a spherically shaped gold sample that covered the entire neutron beam. In this configuration, the total neutron fluence could be determined with an uncertainty of 1.4% by the ratio of the induced γ activities of ^{198}Au and ^{7}Be without any further normalization.

In astrophysics applications, the accurate result of the activation measurement [4] has been used to normalize the energy-dependent Au(n,γ) cross section of Macklin [3] to define a reference cross section that was adopted in numerous measurements for quantitative s-process studies as described in Ref. [7].

There is also a discrepancy of the same magnitude between the results of most measurements of the ^{238}U$(n,\gamma)/^{197}$Au(n,γ) cross-section ratio by means of the TOF technique using the prompt γ registration method and the ratio obtained in the combined fit of the standard. Both discrepancies can only be resolved with new measurements based on different methods and detectors [8,9].

An innovative approach for an absolute measurement of the cross-section ratios ^{238}U$(n,\gamma)/^{197}$Au(n,γ), ^{235}U$(n,\gamma)/^{197}$Au(n,γ), and ^{235}U$(n,\gamma)/^{238}$U(n,γ) is being pursued by activation of natural uranium samples at various keV energies and subsequent accelerator mass spectrometry (AMS) measurements of the reaction products ^{236}U and ^{239}Pu, respectively [10].

This work is part of a new attempt to measure the ^{197}Au (n,γ) cross section via TOF at the n_TOF (neutron time of flight) facility at the European Organization for Nuclear Research (CERN). Two different detection systems for the prompt γ rays emitted in capture events have been used in the experiment, an optimized pair of C_6D_6 (where D denotes ^{2}H) scintillators for the energy range from 1 eV to 1 MeV and a 4π BaF_2 total absorption calorimeter for the region below about 20 keV. Recently, partial results have been published for the resolved resonance region below 5 keV [11], showing excellent agreement between the values obtained with both techniques.

*Corresponding author: claudia.lederer@univie.ac.at
†Deceased.
‡www.cern.ch/ntof

The present study deals with the analysis of the C_6D_6 measurement in the unresolved region up to 400 keV neutron energy. The experiment was designed with the aim of reducing systematic uncertainties as far as possible by using an advanced detector concept and a data acquisition system based on fast digitizers for flexible data analysis. Experimental information on systematic effects was collected in a series of background runs with a lead sample, and comprehensive Monte Carlo (MC) simulations were carried out to validate the remaining corrections.

II. MEASUREMENT

The time-of-flight facility n_TOF at CERN started operation in 2002 with a series of neutron cross-section measurements of interest for nuclear astrophysics and nuclear-waste transmutation. At n_TOF, neutrons are produced via spallation reactions of a pulsed proton beam on a massive lead block of $80 \times 80 \times 60$ cm^3. The high proton momentum of 20 GeV/c, the comparably short pulse width of 7 ns, and an intensity of 7×10^{12} protons per pulse make n_TOF one of the most luminous neutron sources worldwide. By moderation of the initially very energetic neutrons in the 5.8-cm-thick layer of cooling water surrounding the target, a white neutron spectrum ranging from thermal up to several GeV can be used in the experiments. A detailed description of the facility can be found in Refs. [12] and [13].

The experimental area at a flight path of approximately 185 m is connected with the neutron target by an evacuated beam pipe. The intense radiation produced by the impact of the proton beam is strongly reduced by massive iron and concrete shielding walls along the beam pipe and by a 1.5 T magnet for removing charged particles from the beam. The beam profile is shaped by collimators at 140 m and in front of the experimental area at 176 m to the Pb target. For capture studies the diameter of the second collimator is reduced to 1.8 cm, resulting in a neutron beam of about 4 cm in diameter at the position of the capture setup.

Two complementary setups for neutron capture measurements are used at n_TOF, a 4π BaF_2 array [14] acting as a total absorption calorimeter (TAC) for the prompt capture γ rays and a pair of C_6D_6 liquid scintillators. The present measurement was performed with the C_6D_6 detectors because their faster response allows covering the complete energy range up to 1 MeV, whereas the longer recovery time after the γ flash is limiting the presently accessible energy range of the TAC below about 20 keV. At energies above several hundred keV (dependent on the measured isotope) the discrimination against γ rays from inelastic scattering becomes increasingly difficult.

The C_6D_6 detectors are optimized with respect to the lowest possible background from scattered neutrons. This is achieved by using a thin-walled carbon fiber cell for the scintillator that is directly glued onto the photomultiplier and by avoiding any other materials around the detector. In this way, the sensitivity to neutrons scattered by the sample is very low, resulting in an efficiency ratio for the two detectors of $\varepsilon_n/\varepsilon_\gamma \approx 3 \times 10^{-5}$, as demonstrated by Plag *et al.* [15].

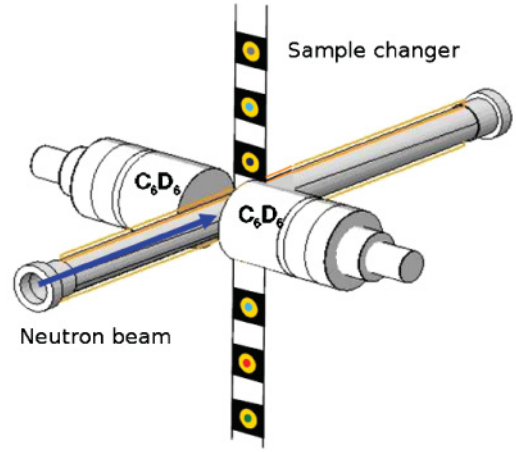

FIG. 1. (Color online) Sketch of sample changer and detectors in the experimental area at a flight path of 185 m.

The schematic sketch of the experiment in Fig. 1 shows the neutron beam line, the C_6D_6 detectors, and the ladder of a remotely operated sample changer. The evacuated beam pipes were stainless steel tubes (wall thickness of 0.5 mm) with 75-μm-thick Kapton windows. To avoid angular distribution effects for resonances with $\ell > 0$ and to reduce the background due to in-beam γ rays from neutron captures in the water moderator [12], which are scattered by the sample preferentially in forward direction, the detectors were mounted 9.5 cm upstream of the sample, corresponding to an effective angle of 125° relative to direction of the neutron beam.

The gold sample was 15.02 mm in diameter and 0.38 mm in thickness. It was glued glued onto a 75-μm-thick Kapton foil sustained by a carbon fiber frame, which was always outside of the neutron beam. A lead sample was used for determining the neutron-induced backgrounds (e.g., from neutrons scattered on the sample) and the in-beam γ-ray background (Table I). An empty position on the sample ladder served for measuring the sample-independent background.

The detector signals have been recorded with fast digitizers at a sampling rate of 500 MHz, corresponding to time steps of 2 ns/sample. Triggered by the pickup signal of the accelerator, each neutron burst could be followed for 16 ms by intermediate data storage in the 8-MB onboard memory of the digitizers. Thus, the effective neutron energy range covered in this measurement spans from 0.7 eV up to 1 MeV. The lowest energy corresponds to the largest time-of-flight of 16 ms, which can be acquired in the 8-MB buffer of the flash analog-to-digital converters, whereas the 1 MeV limit is due to the recovery time of the setup from the γ flash. The time zero point in the TOF spectrum was derived from the γ flash on an

TABLE I. Sample characteristics.

Sample	Mass (mg)	Thickness (10^{-3} atoms/b)	Diameter (mm)	Chemical form
Au	1299.0	2.243	15.02	metal
^{nat}Pb	2027.0	3.173	15.38	metal

event-by-event basis. For events following the γ flash, TOF, pulse height, and integrated charge were determined by an off-line analysis routine. This raw information was converted into preprocessed data by energy calibration of the scintillators, verification of gain stability, selection of proper thresholds, and rejection of coincident events [16]. The digitizers were operated with lower energy thresholds of 160 keV. During data processing, a common threshold of 200 keV was adopted, and an additional threshold of 8 MeV was applied to eliminate high-energy background events.

The transformation from time of flight to neutron energy is related to both the flight length and the energy-dependent resolution function. We have adopted the TOF-energy relation from Ref. [17].

A neutron monitor consisting of a ^{6}Li layer of 200 μg/cm^2 in thickness evaporated onto a 1.5-μm-thick Mylar foil was mounted about 3.5 m upstream of the capture samples for additional flux measurements. The products of the ^{6}Li$(n,\alpha)^3$H reaction were recorded by four silicon detectors surrounding the ^{6}Li foil outside the neutron beam [18]. Furthermore, the neutron flux had been measured by means of a calibrated parallel-plate fission chamber with a ^{235}U deposit provided by Physikalisch-Technische Bundesanstalt Braunschweig [19].

III. DATA ANALYSIS

A. Determination of the capture yield

The efficiency of C_6D_6 scintillators for detecting the prompt γ-ray cascade emitted in neutron capture reactions depends in a complex way on the deexcitation path of the compound nucleus. Therefore, the measured signals have to be subjected to the PHWT [5], an *a posteriori* manipulation of the detector response to ensure that the γ-ray efficiency increases linearly with the detector signal. Under that condition the efficiency for detecting a capture event becomes proportional only to the excitation energy, $\epsilon_C = c * E_C = c * (S_n + E_n)$, which is defined as the sum of the neutron separation energy S_n and the neutron kinetic energy E_n.

The experimental capture yields are obtained by means of weighting functions (WF), which are parametrized as polynomial functions of the γ-ray energy. Each recorded detector event is weighed by the proper WF to make the cascade efficiency of the detectors proportional to the excitation energy. This manipulation of the raw data is valid if the efficiency of the detector is low enough to detect only one γ ray per capture event, which is the case for the C_6D_6 setup.

An accuracy of 2% was determined for the PHWT by a detailed study of the possible sources of systematic uncertainties [20]. The PHWT requires coincidence rejection, reliable energy calibration of the γ-ray detection, and a detailed simulation of the experimental setup to determine the WFs.

The WFs have been determined using calculated response functions for monoenergetic γ rays, which were obtained by means of detailed MC simulations of the experimental setup with GEANT4 [21] and MCNPX [22]. The three-dimensional spatial distribution of primary γ rays is generated using the neutron beam profile for the radial dimension [23] and the neutron absorption probability across the sample thickness, which obviously depends on the particular value of the cross section and, therefore, on neutron energy. In this way, the self-absorption effect of the γ rays in the sample is realistically considered. This approach has been described in detail in the preceding n_TOF analysis of the resolved resonance region [11] together with the justification for the 2% uncertainty taken in this work. The same procedure was also used in previous works [20,24–28].

After application of the WFs the capture yield is obtained as

$$Y = \frac{1}{A} f_{\rm ms} \frac{(C_{\rm w} - B_{\rm w})}{\Phi E_{\rm c}}, \quad (1)$$

where A is the fraction of the neutron beam covering the sample (see Sec. III D), $C_{\rm w}$ is the weighted, dead-time-corrected energy spectrum, $B_{\rm w}$ is the weighted background, Φ is the net neutron flux, and $E_{\rm c}$ is the excitation energy. The dead time is taken into account by putting a veto of 30 ns, slightly larger than the system dead time, between two consecutive signals. This results in a well-defined dead time, for which we correct (correction on the order of a few per mil).

Since in the present case the measurement is self-normalized to the 4.9-eV resonance, additional corrections, e.g., the energy threshold applied to the deposited γ energy or the creation of conversion electrons, are not necessary, assuming that the decay spectra of the compound nucleus are similar for different neutron energies. This has been verified by analyzing the data using different energy thresholds and comparing the resulting capture yields. The sample-related correction $f_{\rm ms}$ for neutron multiple scattering and neutron self-shielding was calculated with the code SESH [29]. As shown in Fig. 2, $f_{\rm ms}$ is always smaller than 4% in the considered energy range. Assuming a conservative value for the uncertainty of 10%, this correction will enter into the final uncertainty with 0.4%.

For the flux we used a modeled version of the standard flux of n_TOF phase I [30]. This flux represents the total number of incoming neutrons per pulse crossing the plane at the sample position and needs to be corrected by the fraction intercepted by the sample, which is the energy-dependent fraction $A(E)$

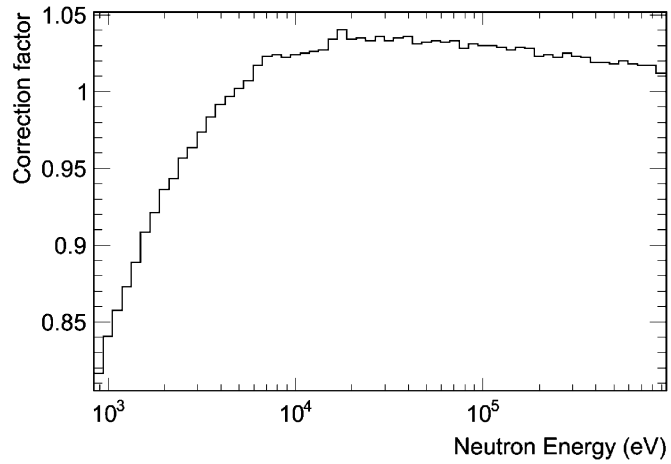

FIG. 2. Correction factor for multiple scattering and self-shielding calculated with the code SESH [29].

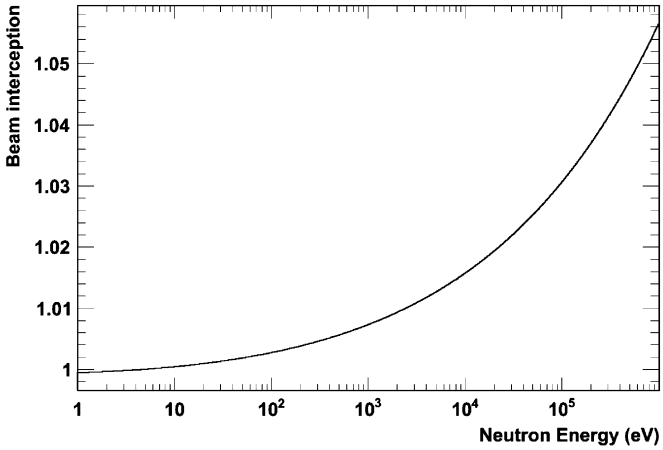

FIG. 3. The fraction of the neutron beam covered by a sample that is 15 mm in diameter relative to the value applied at the saturated resonance at 4.9 eV.

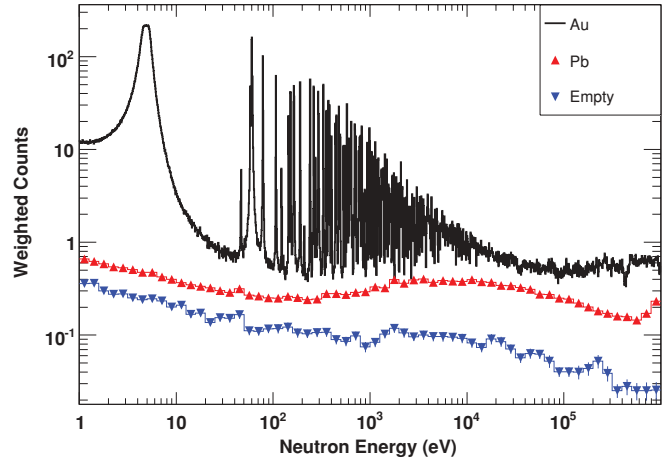

FIG. 4. (Color online) Weighted Au spectrum compared to runs with Pb and with an empty position in the sample ladder.

of Eq. (1). The beam profile in different energy regions has been simulated (2%–4% uncertainty) and is in agreement with corresponding measurements [23]. This factor relative to the value at 4.9 eV is plotted in Fig. 3 for a sample that is 15 mm in diameter. The same factor was used in previous measurements of ^{232}Th [31], which were in excellent agreement with results for ^{232}Th obtained at Geel Linear Accelerator (GELINA) [32]. The uncertainty on the beam profile correction factor is negligible.

B. Background components

The background in the keV region is essentially determined by elastic neutron scattering and by the contributions due to in-beam γ rays. These components were determined experimentally in dedicated runs with a lead sample. Additional measurements with neutron filters have been made for normalization of these background runs. The sample-independent background was obtained with an empty position in the sample ladder. The individual spectra are shown in Fig. 4. The effect of sample activation was practically negligible thanks to the highly intense neutron pulses of the n_TOF facility.

The contribution of the neutron-induced background and (to a lesser extent) the sample-independent background measured without sample exhibit a smooth decrease close to a $1/v$ dependence with neutron energy. The background reduces to this component below 200 eV.

Between 200 and 500 keV the detection of in-beam γ rays, which are scattered in the sample, represents the main background contribution. These γ rays originate mostly from neutron captures in the cooling water or in the spallation target during and after the moderation process and reach the experimental area at the same time as neutrons in the energy range between 1 and 100 keV. The photon energy spectrum, which exhibits a prominent peak at 2.2 MeV from capture events in hydrogen, extends up to several MeV [12] and is energetic enough to be registered with considerable efficiency above the 200 keV threshold used in data analysis.

It turned out that the spectrum taken with the Pb sample shown in Fig. 5 was particularly useful for characterizing both background components described above because the capture cross section of Pb is extremely low compared to that of Au and is almost free of resonances in the energy range of interest, whereas the cross section for neutron elastic and γ scattering is similar to that of gold.

At high energies, γ rays produced by inelastic neutron scattering add another background component, which was investigated by increasing the energy threshold from the nominal 200 keV to 1 MeV. The comparison of both spectra in Fig. 6 exhibits good agreement up to 600 keV. The small discrepancies in the 10–80 keV region are due to the small remaining in-beam γ background in the 1-MeV spectrum where a proper subtraction due to low statistics is not possible.

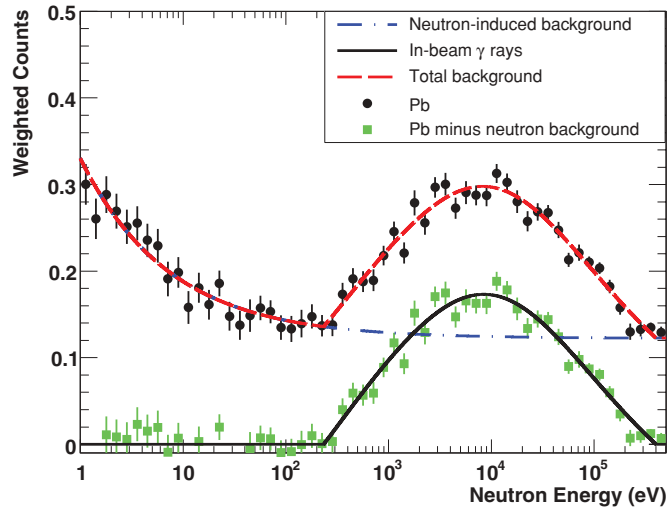

FIG. 5. (Color online) Decomposition of the spectrum measured with the Pb sample into the close to $1/v$ dependence of the neutron-scattering background and the contribution from in-beam γ rays.

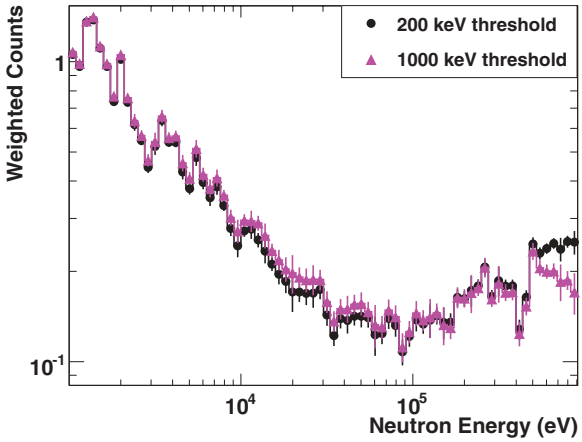

FIG. 6. (Color online) Normalized weighted counts obtained with the nominal γ-ray threshold of 200 keV and with a threshold of 1 MeV. The effect of the inelastic channel appears at energies of about 600 keV.

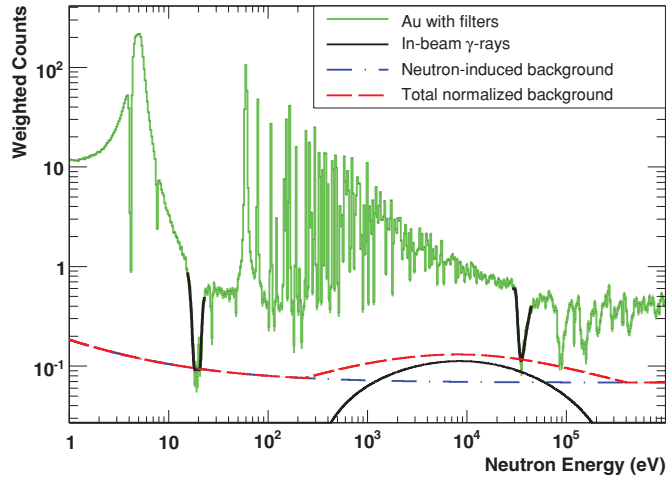

FIG. 7. (Color online) Au spectrum with filters in the neutron beam. The two background components B_n and B_γ have been fitted to match the minimum of the filter dips.

C. Background shape and normalization

Once the neutron energy dependence of both neutron-induced and in-beam γ-ray components have been accurately characterized (see Sec. III B), the total background can be expressed as

$$B(E_n) = f_n\, B_n(E_n) + f_{att}\, f_\gamma\, B_\gamma(E_n), \quad (2)$$

where the terms B_n and B_γ describe the background shape due to different background components and f_n and $f_{att}\, f_\gamma$ are the respective factors for normalizing these components to the Au measurement. We parametrized the neutron-induced and in-beam γ-component $B_n(E_n)$ and $B_\gamma(E_n)$ as

$$B_n(E_n) = a + b/\sqrt{E_n} \quad (3)$$

and

$$B_\gamma(E_n) = c + d\exp(-e/\sqrt{E_n}) + f\exp(g/\sqrt{E_n}). \quad (4)$$

The exponential terms in Eq. (4) represent the production and decay of activation products in the spallation target.

Values for a and b were determined by a least-squares fit of the Pb spectrum from 1 to 100 eV and at 500 keV, where the in-beam γ background disappears again. After subtracting the resulting neutron-induced background from the Pb spectrum, the coefficients c to g were fitted to the remaining part (Fig. 5).

To normalize these background components, a spectrum of the Au sample was taken with filters in the neutron beam downstream of the first collimator [33]. The thickness of the filters (30 mm for Al and 0.8 mm for W) was chosen such that neutrons were completely removed at the position of black resonances at 20.06 eV in W and at 34.7 keV in Al. The Au spectrum taken with filters was first corrected for the overall flux attenuation in the filters. The normalization factors f_n and f_γ for the neutron-induced and in-beam γ-ray components were then determined such that the sum of the background components matched the filter dips, as shown in Fig. 7.

The best fit values were found for $f_n = 0.558 \pm 0.033$ and $f_\gamma = 0.354 \pm 0.017$. The uncertainties were evaluated by considering the counting statistics in the filter dips and the fit of the filter transmission with a single-level Breit-Wigner shape and by repeated fits using different energy bin widths.

The factor f_{att} accounts for the attenuation of in-beam γ rays in the filters. It was determined by a series of GEANT3 [34] simulations based on the in-beam γ-ray spectrum from Ref. [12] and on a detailed replica of the experimental setup. The simulated events were analyzed in the same way as the real data, with a threshold of 200 keV on the deposited energy in the C_6D_6 detectors. The correction for the γ attenuation in the W and Al filters was 1.83 ± 0.08, where the uncertainty in the simulation was mostly due to the effect of the detection threshold.

In addition, the background was also investigated in a second approach by determining the scaling factor of the in-beam γ background by Monte Carlo simulations using GEANT3 and MCNPX. The simulations of the gamma interaction in the Pb and the Au samples and their subsequent detection in the C_6D_6 scintillators were performed using the spectrum of the in beam gamma rays and a detailed description of the experimental setup and samples as input. The scaling factors obtained from the simulations were 0.625 (GEANT3) and 0.658 (MCNPX), thus in excellent agreement with each other and with the corresponding value $f_{att}\, f_\gamma = 0.648$ found by the method previously described. Hence, $f_{att}\, f_\gamma$ was adopted with 0.648 ± 0.032, estimating an uncertainty of 5%. The resulting uncertainty of the background varies with neutron energy and peaks at the minimum of the signal/background ratio near 30 keV. Thanks to a signal/background ratio of 3–10, the contribution to the uncertainty of the cross section amounts to 0.6%–1.7% in the energy range of the experiment (see also Table II).

D. Normalization of the capture yield

The neutron capture yield is self-normalized since the 4.9 eV resonance is saturated for the thickness of the used sample. The normalization was obtained by fitting the top of this resonance with the R-matrix code SAMMY [35]. The

TABLE II. Systematic and statistical uncertainties at different energies.

Source of uncertainty	Uncertainty (%)		
	10 keV	30 keV	100 keV
PHWT		2.0	
Neutron flux shape		2.0	
Normalization		1.0	
Sample geometry		0.5	
Background subtraction	1.0	1.5	1.3
Multiple scattering and self shielding	0.3	0.4	0.3
Counting statistics[a]	3.0	4.4	3.7
Total	4.4	5.6	5.0

[a]For a resolution of 20 bins per decade.

uncertainty of the normalization is estimated as being 1.0%. However, the used weighting function may be different in a saturated resonance because the capture γ rays originate only in a thin layer of the sample instead of throughout the sample in the unresolved resonance region. The size of this effect and the corresponding correction factor depend on the details of the detector-sample geometry and can be obtained by Monte Carlo simulations of the weighting function, modeling either a thin layer or a homogeneous gamma source inside the sample [24]. In the present geometry, the effect was 0.6%; hence, the yield was scaled by the factor 1.006.

E. Uncertainties

The uncertainties related to the various steps of data analysis have been discussed throughout the previous subsections. These contributions are summarized in Table II for three representative neutron energies to illustrate the relatively weak effect of the energy-dependent components. The comparison shows that the present systematic uncertainty is dominated by the energy dependence of the neutron flux and the PHWT. Imperfections in the sample shape introduce an additional systematic uncertainty of 0.5%.

IV. RESULTS

A. Comparison with evaluations and previous data

The neutron capture cross section of ^{197}Au was measured from 5 to 400 keV with an overall uncertainty of 3.9%–6.7%. Although the energy range was extending to about 1 MeV, the data given here are restricted to the region below 400 keV because the uncertainties of the present data are increasing at higher energies and did not provide meaningful constraints for the standard. The results are given in Table III with a resolution of 20 bins per decade. The comparison with evaluated cross sections transformed to 20 bins per decade in Fig. 8 shows good agreement with the Evaluated Nuclear Data File Version B-VII.0 (ENDF/B-VII.0) [36], which contains the standard evaluation, as well as with the Japanese Evaluated Nuclear Data Library Version 4.0 (JENDL-4.0) [37] and the Joint Evaluated Fission and Fusion File Version 3.1 (JENDL-3.1) [38]. From 200 to 400 keV, where the Au(n,γ) cross section

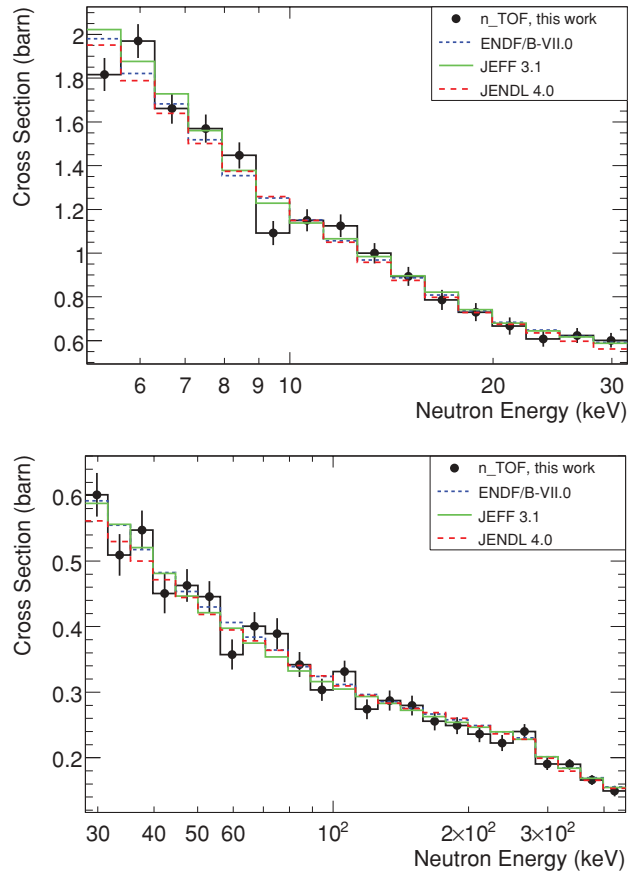

FIG. 8. (Color online) Comparison of present results with a resolution of 20 bins per decade with evaluated data sets from the ENDF/B-VII.0 [36], JEFF-3.1 [38], and JENDL-4.0 [37] libraries.

is an accepted standard, the agreement is within quoted uncertainties for all energy bins except the regions from 223 to 251 keV and from 282 to 316 keV, where the deviations are 5.3% and 7.3%, respectively. When averaging the cross section from 200 to 400 keV, the agreement with the standard is 2.1%.

In view of the discrepancy between the ENDF evaluation and the accurate cross sections reported by Macklin *et al.* [2,3] and by Ratynski and Käppeler [4], the following discussion concentrates on these measurements. The comparison with the first of these data sets is particularly illustrative because the energy-dependent cross section provides a more stringent test compared to the spectrum-averaged result. In Fig. 9, the present results and the data of Refs. [2,3] are plotted with the same binning to facilitate the direct comparison. Also, the ratio of the two data sets is shown. While the top and middle panels shows that the cross sections obtained in this work are systematically higher up to 100 keV, the zoom into the region from 8 to 40 keV with a resolution of 250 bins per decade in the bottom panel demonstrates that the cross-section fluctuations reported by Macklin *et al.* [2,3] are quantitatively confirmed by the present data. The origin of these structures is discussed in Sec. IV B.

Furthermore, we calculated the Maxwellian-averaged cross sections (MACS) from 5 keV to 100 keV using the code SAMMY. For energies below 5 keV we used resonance

TABLE III. ^{197}Au(n,γ) cross sections and overall uncertainties.

E_{low} (keV)	E_{high} (keV)	σ (mb)	Uncertainty (%)		
			Statistic	Systematic	Total
5.010	5.621	1817	2.7	3.1	4.1
5.621	6.307	1970	2.4	3.1	3.9
6.307	7.076	1661	2.7	3.1	4.1
7.076	7.940	1569	2.6	3.1	4.1
7.940	8.908	1447	2.7	3.2	4.1
8.908	9.995	1092	3.8	3.2	5.0
9.995	11.215	1150	3.0	3.2	4.4
11.215	12.583	1125	3.3	3.2	4.6
12.583	14.119	1000	3.3	3.2	4.7
14.119	15.842	894	3.6	3.3	4.8
15.842	17.775	786	4.7	3.3	5.8
17.775	19.943	730	4.6	3.4	5.7
19.943	22.377	666	4.9	3.4	6.0
22.377	25.107	608	4.8	3.4	5.9
25.107	28.171	623	4.2	3.4	5.4
28.171	31.608	601	4.4	3.4	5.6
31.608	35.465	509	5.2	3.6	6.3
35.465	39.792	547	4.2	3.5	5.5
39.792	44.648	450	5.7	3.5	6.7
44.648	50.096	463	4.1	3.4	5.4
50.096	56.208	446	4.2	3.4	5.4
56.208	63.067	357	5.4	3.5	6.4
63.067	70.762	400	4.2	3.3	5.4
70.762	79.396	389	5.1	3.3	6.1
79.396	89.084	342	4.4	3.4	5.6
89.084	99.954	304	4.3	3.4	5.5
99.954	112.150	332	3.7	3.3	5.0
112.150	125.835	274	4.3	3.3	5.5
125.835	141.189	287	4.3	3.3	5.4
141.189	158.416	280	4.3	3.3	5.4
158.416	177.746	256	4.4	3.3	5.5
177.746	199.434	249	4.0	3.2	5.2
199.434	223.769	236	4.1	3.2	5.2
223.769	251.073	222	4.6	3.2	5.6
251.073	281.709	240	3.5	3.2	4.7
281.709	316.082	191	3.8	3.2	4.9
316.082	354.650	190	2.9	3.2	4.3
354.650	397.924	166	3.3	3.2	4.6

parameters determined at n_TOF in the same experiment, published in Ref. [11]; above 400 keV we used the ENDF/B-VII.0 cross section. This allows a direct comparison to the MACS at 30 keV given by Ratynski and Käppeler. In Table IV the Maxwellian-averaged cross sections are listed from 5 to 100 keV. The contributions from the regions below 5 and above 400 keV, which are not covered by the present results, are indicated separately. The total uncertainty of the MACS ranges from 3.1% to 3.6% since it is dominated by systematic uncertainties. In the unresolved resonance region we see a contribution of 0.7% to the MACS uncertainty due to counting statistics. Because the cross section increases toward lower energies, it is safe to assume that the statistical uncertainty becomes smaller as well. Therefore, we adopt a 0.7% uncertainty for the fraction of the resolved resonance region as a conservative estimate. The systematic uncertainties on the MACS range from 3.0% to 3.5%.

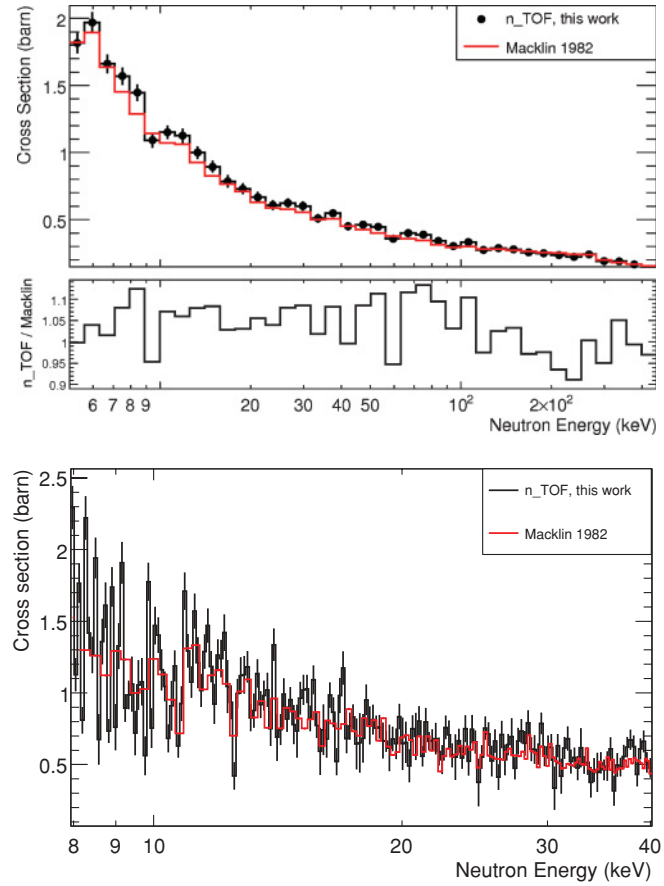

FIG. 9. (Color online) (top) The present results compared to the data of Macklin *et al.* [2,3] for the full energy range from 5 to 400 keV (20 bins per decade). (middle) Results divided by the data of Macklin *et al.* (bottom) Comparison of present results with the data of Macklin *et al.* in the energy region from 8 to 40 keV (250 bins per decade, with the original binning of Refs. [2,3]) to highlight the pronounced cross-section fluctuations. Uncertainties shown for n_TOF data in the bottom panel are statistical.

The MACS at 30 keV is 582 ± 9 mb, according to Ratynski and Käppeler [4], while the present data yield a MACS of 611 ± 22 mb, which is 4.7% higher. In Fig. 10 a comparison between selected experimental data and the two evaluations ENDF/B-VII.0 and JEFF-3.1 is shown. Our data show perfect agreement with Kazakov *et al.* [39] and the evaluations and are also still in fair agreement with Refs. [2–4,40–44].

B. Gross structures

From the average level spacing of $l = 0$ states in ^{198}Au above the neutron binding energy ($\langle D_0 \rangle = 16.5 \pm 0.9$ eV) and from the width of these compound states (of the order of 0.3 eV at 10 keV) it is obvious that the significant structures in the capture cross section of Au (Figs. 8 and 9) are certainly not due to single resonances. Likewise, structures in the neutron flux can be excluded as a possible explanation because these are much smaller and are not at all correlated with those seen in the gold data.

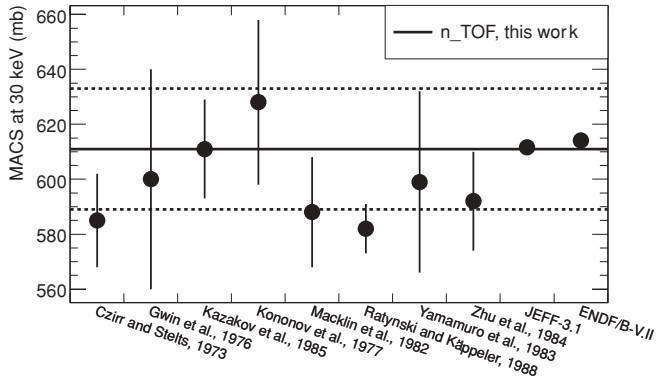

FIG. 10. Comparison of the Maxwellian-averaged cross section at 30 keV (dashed lines indicates 1σ uncertainty) with selected experimental data [2–4,39–44] and the evaluations ENDF/B-VII.0 and JEFF-3.1. Data are taken from Ref. [45]

The origin of these structures has been investigated by simulations using artificial sets of resonances with realistic statistical properties, which were obtained from the observed average level spacings $\langle D_0 \rangle$, neutron strength function ($S_0 = 1.9 \times 10^{-4}$), and average γ-ray width ($\langle \Gamma_\gamma \rangle = 0.128 \pm 0.006$ eV) assuming a $(2J + 1)$ dependence of the level density. Based on the standard Fermi-gas model, this yields 454 and 758 levels in the range from 0 to 20 keV for $J = 1$ ($\langle D_0 \rangle = 44.1$ eV) and $J = 2$ ($\langle D_0 \rangle = 26.4$ eV), respectively. The statistical properties of each set are compatible with a Wigner distribution of the level spacings, a Porter-Thomas distribution of neutron widths, and a constant or Gaussian distribution of the gamma widths.

TABLE IV. Maxwellian-averaged cross sections of ^{197}Au(n,γ) from 5 to 100 keV with total uncertainties. Contributions outside of the investigated energy range are listed separately.

$k_B T$ (keV)	MACS (mb)	Contribution to MACS (%)	
		$E_n < 5$ keV	$E_n > 400$ keV
5.0	1970 ± 70	49.6	–
6.0	1729 ± 61	42.2	–
7.0	1550 ± 54	36.5	–
8.0	1412 ± 49	32.0	–
9.0	1302 ± 46	28.3	–
10.0	1212 ± 42	25.3	–
12.5	1044 ± 37	19.7	–
15.0	927 ± 33	15.9	–
17.5	841 ± 30	13.2	–
20.0	775 ± 27	11.2	–
25.0	678 ± 24	8.4	–
30.0	611 ± 22	6.6	–
35.0	560 ± 20	5.3	–
40.0	521 ± 18	4.4	–
45.0	490 ± 17	3.7	0.1
50.0	464 ± 16	3.2	0.2
60.0	423 ± 14	2.5	0.5
70.0	392 ± 13	2.0	1.2
85.0	357 ± 12	1.5	2.9
100.0	330 ± 10	1.2	5.2

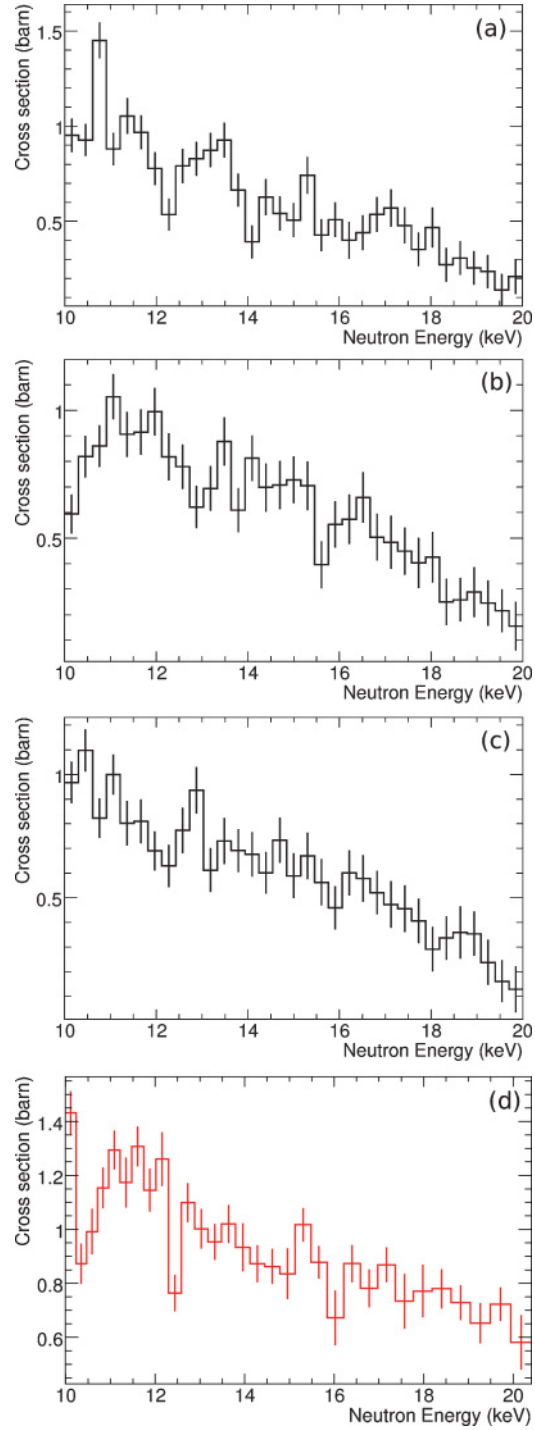

FIG. 11. (Color online) (a–c) Simulated cross sections compared to (d) experimental data in the region between 10 and 20 keV. Uncertainties shown for n_TOF data are statistical.

The pointwise cross-section data calculated with the multilevel Breit-Wigner formalism using the PREPRO code [46] are Doppler broadened with $T = 300$ K and $T = 4560$ K. The higher temperature was chosen because it corresponds to the n_TOF resolution in the neutron energy range from 10 to

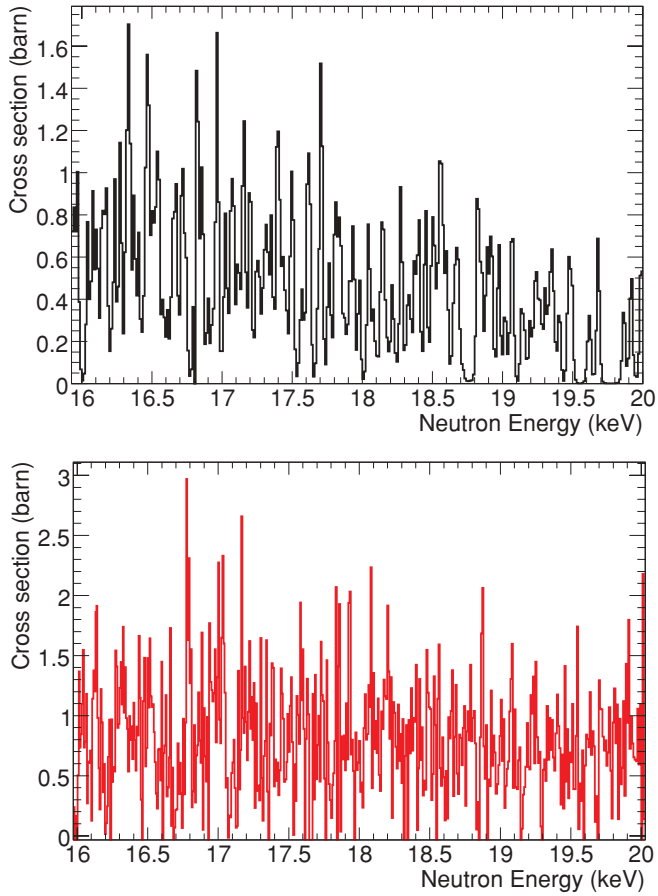

FIG. 12. (Color online) The same comparison as in Fig. 11 (top: simulation; bottom: experiment) but using a bin width of 7 eV, about 3 times smaller than the experimental resolution of 22 eV at 17.5 keV. This confirms that the cross section fluctuations are observed independently of the bin width, thus providing additional evidence for their real existence.

20 keV (FWHM ≈ 18 eV). The calculated spectra with three sets of simulated resonances are compared in Fig. 11 with the experimental cross section using a resolution of 100 bins per decade.

Three different sets of simulations have been performed, resulting in three completely different sets of resonances, which exhibit fluctuations corresponding to the experimentally observed structures. The error bars are estimated assuming a statistical uncertainty of $N^{-0.5}$ for N events in the bin. Although no real agreement with the experimental data is to be expected, the simulated fluctuation properties are clearly compatible with the structures in the cross section. This supports the adopted interpretation that they reflect the density of compound states at excitation energies of 10–20 keV above the neutron separation energy. If the data are plotted with much finer binning, the comparison with the simulations confirms the real nature of the structure. This is illustrated in Fig. 12, where the bin width of ≈7 eV is considerably smaller than the experimental resolution of 22 eV at 17.5 keV neutron energy.

V. SUMMARY AND CONCLUSIONS

The neutron capture cross section of ^{197}Au has been measured at n_TOF/CERN over the wide energy range from 1 eV to 400 keV. Following a detailed resonance analysis [11], this work deals with the unresolved region starting at 5 keV. Based on a thorough study of the various background components and on the careful evaluation of the uncertainties, the cross section was derived with an accuracy of 3.9%–6.7% on a grid of 20 bins per energy decade (Table III). The data set with full resolution is available in the EXFOR database [47]. In the critical energy range below 200 keV the present results are in fair agreement with the standard evaluation, while being systematically higher by few percent than the TOF measurement of Macklin *et al.* [2,3].

Maxwellian-averaged cross sections from 5 to 100 keV have been extracted with an uncertainty from 3.1% to 3.6%. A comparison of the MACS at 30 keV shows good agreement with other experimental data and is 4.7% higher than the MACS determined in the activation study of Ratynski and Käppeler [4].

The structures in the ^{197}Au cross section have been investigated by simulation of the expected level density using average resonance properties deduced from the resolved resonance region. It could be shown that the experimental evidence for such structures was confirmed by the gross features of the simulated data. Accordingly, these structures are physically relevant and could be included in a future evaluation.

In light of the accuracy, the high-energy resolution, and the wide energy range of the present results, it appears likely that the goal of establishing the ^{197}Au(n,γ) cross section as a standard in the keV region can soon be reached. The comparison with the most accurate previous data shows fair agreement within the actual uncertainties. Nevertheless, further efforts to resolve the remaining differences would be most welcome, either by current TOF work at other facilities [48] or by additional activation studies [49,50]. In this context, recent improvements of the n_TOF facility, which led to a reduction of the in-beam γ background by an order of magnitude [51], also bear promising options for complementary improvements.

[1] A. D. Carlson *et al.*, Nucl. Data Sheets **110**, 3215 (2009).
[2] R. L. Macklin, J. Halperin, and R. R. Winters, Phys. Rev. C **11**, 1270 (1975).
[3] R. Macklin, private communication to S. F. Mughabghab, 1982; see also [www.nndc.bnl.gov/nndc/], EXFOR 12720.002 (unpublished).
[4] W. Ratynski and F. Käppeler, Phys. Rev. C **37**, 595 (1988).
[5] R. L. Macklin and R. H. Gibbons, Phys. Rev. **159**, 1007 (1967).
[6] M. Busso, R. Gallino, and G. Wasserburg, Annu. Rev. Astron. Astrophys. **37**, 239 (1999).
[7] F. Käppeler, R. Gallino, S. Bisterzo, and W. Aoki, Rev. Mod. Phys. (in press).
[8] V. G. Pronyaev, A. Mengoni, and A. D. Carlson, Technical Report INDC(NDS)-0540, IAEA, Vienna, 2008.

[9] A. D. Carlson *et al.*, in *Nuclear Data for Science and Technology* 2010 (in preparation).

[10] A. Wallner, T. Belgya, M. Bichler, K. Buczak, I. Dillmann, F. Käppeler, A. Mengoni, F. Quinto, P. Steier, and L. Szentmiklosi, "*Neutron capture studies on 235U and 238U via AMS*", accepted, Nuclear Engineering and Technology (2011).

[11] C. Massimi, C. Domingo Pardo *et al.* (n_TOF Collaboration), Phys. Rev. C **81**, 044616 (2010).

[12] U. Abbondanno (n_TOF Collaboration) Technical Report CERN-SL-2002-053 ECT, CERN, Geneva, 2003.

[13] F. Gunsing *et al.*, Nucl. Instrum. Methods Phys. Res., Sec. B **361**, 925 (2007).

[14] C. Guerrero *et al.*, Nucl. Instrum. Methods Phys. Res., Sec. A **608**, 424 (2009).

[15] R. Plag *et al.*, Nucl. Instrum. Methods Phys. Res., Sec. A **496**, 425 (2003).

[16] M. Mosconi, Ph.D. thesis, University of Karlsruhe, 2007.

[17] G. Lorusso *et al.*, Nucl. Instrum. Methods Phys. Res., Sec. A **532**, 454 (2004).

[18] S. Marrone *et al.*, Nucl. Instrum. Methods Phys. Res., Sec. A **517**, 289 (2004).

[19] C. Borcea *et al.*, Nucl. Instrum. Methods Phys. Res., Sec. A **513**, 524 (2003).

[20] U. Abbondanno *et al.*, Nucl. Instrum. Methods Phys. Res., Sec. A **521**, 454 (2004).

[21] S. Agostinelli *et al.* (Geant4 Collaboration), Nucl. Instrum. Methods Phys. Res., Sec. A **506**, 250 (2003); see also [www.geant4.org/geant4/].

[22] J. F. Briesmeister, Los Alamos National Laboratory Report LA-13709-M, 2000; see also [http://mcnpx.lanl.gov].

[23] J. Pancin *et al.*, Nucl. Instrum. Methods Phys. Res., Sec. A **524**, 102 (2004).

[24] A. Borella, G. Aerts, F. Gunsing, M. Moxon, P. Schillebeeckx, and R. Wynants, Nucl. Instrum. Methods Phys. Res., Sec. A **577**, 626 (2007).

[25] C. Domingo-Pardo *et al.* (n_TOF Collaboration), Phys. Rev. C **74**, 025807 (2006).

[26] C. Domingo-Pardo *et al.* (n_TOF Collaboration), Phys. Rev. C **74**, 055802 (2006).

[27] C. Domingo-Pardo *et al.* (n_TOF Collaboration), Phys. Rev. C **75**, 015806 (2007).

[28] C. Domingo-Pardo *et al.* (n_TOF Collaboration), Phys. Rev. C **76**, 045805 (2007).

[29] F. H. Fröhner, SESH computer code, GA-8380, Gulf General Atomic, San Diego, California (1968).

[30] C. Borcea *et al.* Nucl. Instrum. Methods Phys. Res., Sec. A **513**, 524 (2003).

[31] G. Aerts *et al.* (n_TOF Collaboration), Phys. Rev. C **73**, 054610 (2006).

[32] A. Borella, K. Volev, A. Brusegan, P. Schillebeeckx, F. Corvi, N. Koyumdjieva, N. Janeva, and A. A. Lukyanov, Nucl. Sci. Eng. **152**, 1 (2006).

[33] D. B. Syme, Nucl. Instrum. Methods Phys. Res. **198**, 357 (1982).

[34] J. Apostolakis, *CERN program library long writeup, W5013*, CERN, GEANT library (1993); see also [http://wwwinfo.cern.ch/asd/geant/].

[35] N. M. Larson, Technical Report ORNL/TM-9179/R7, Oak Ridge National Laboratory, 2003.

[36] M. B. Chadwick *et al.*, Nucl. Data Sheets **107**, 2931 (2006).

[37] K. Shibata *et al.*, J. Nucl. Sci. Technol. **48**, 1 (2011).

[38] A. Koning, R. Forrest, M. Kellett, R. Mills, H. Henriksson, Y. Rugama, JEFF Report 21, OECD/NEA, Paris, 2006; see also [http://www.oecd-nea.org/dbforms/data/eva/evatapes/jeff_31/].

[39] L. Kazakov *et al.*, Technical Report INDC(CCP)-248/G, Institute for Physics and Power Engineering, Oblozinsky, 1985.

[40] N. Yamamuro, M. Igashira, T. Sekiya, and H. Shirayanagi, J. Nucl. Sci. Technol. **20**, 797 (1983).

[41] J. B. Czirr and M. L. Stelts, Nucl. Sci. Eng. **52**, 299 (1973).

[42] R. Gwin, E. G. Silver, R. W. Ingle, and H. Weaver, Nucl. Sci. Eng. **59**, 79 (1976).

[43] V. N. Kononov, B. D. Yurlov, E. D. Poletaev, and V. M. Timokhov, Yad. Fiz. **26**, 947 (1977) [Sov. J. Nucl. Phys. **26**, 500 (1977)].

[44] S. Zhu, S. Jiang, Y. Chen, and D. Luo, Chin. J. Nucl. Phys. **6**, 23 (1984).

[45] I. Dillmann, M. Heil, F. Käppeler, R. Plag, T. Rauscher, and F.-K. Thielemann, in *KADoNiS—The Karlsruhe Astrophysical Database of Nucleosynthesis in Stars*, AIP Conf. Proc. No. 819 (AIP, College Park, MD), p. 123.

[46] ENDF/B Pre-processing codes (PREPRO), [http://www-nds.iaea.org/ndspub/endf/prepro/].

[47] Experimental Nuclear Reaction Data (EXFOR), [http://www-nds.iaea.org/exfor/exfor.htm].

[48] C. Lampoudis, S. Kopecky, C. Massimi, M. Moxon, and P. Schillebeeckx, Standard CM 2010, IAEA, Vienna, 2010; see also [http://www-nds.iaea.org/standards/CM2010/].

[49] Y. Eisen *et al.*, Nuclear Measurements, Evaluations and Applications, NEMEA-6, OECD Nuclear Energy Agency, Paris (in preparation).

[50] C. Lederer, I. Dillmann, U. Giesen, F. Käppeler, A. Mengoni, M. Mosconi, R. Nolte, and A. Wallner, *Definition of a standard neutron field with the ^{7}Li(p,n)^{7} Be reaction*, Final scientific EFNUDAT workshop, CERN, Geneva (in preparation), [http://www.efnudat.eu/workshops.html].

[51] M. Calviani (n_TOF Collaboration), in Slow and Resonance Neutrons: Scientific Workshop on Neutron Measurements, Theory and Applications (Hungarian Academy of Sciences, Budapest, 2010), p. 33 (unpublished), [http://www.efnudat.eu/workshops.html].